PROCEEDINGS A

royalsocietypublishing.org/journal/rspa

Research

Cite this article: Dyachenko AI, Dyachenko SA, Lushnikov PM, Zakharov VE. 2021 Short branch cut approximation in two-dimensional hydrodynamics with free surface. *Proc. R. Soc. A* **476**: 20200811.
https://doi.org/10.1098/rspa.2020.0811

Received: 10 October 2020
Accepted: 29 March 2021

Subject Areas:
applied mathematics, fluid mechanics

Keywords:
hydrodynamics, gravity waves, conformal map

Author for correspondence:
P. M. Lushnikov
e-mail: plushnik@math.unm.edu

Short branch cut approximation in two-dimensional hydrodynamics with free surface

A. I. Dyachenko[1,2], S. A. Dyachenko[3,4], P. M. Lushnikov[1,5] and V. E. Zakharov[1,2,6]

[1]Landau Institute For Theoretical Physics, Moscow, Russia
[2]Center for Advanced Studies, Skoltech, Moscow 143026, Russia
[3]Department of Applied Mathematics, University of Washington, Seattle WA 98195, USA
[4]Department of Mathematics, SUNY Buffalo, Buffalo NY 14260, USA
[5]Department of Mathematics and Statistics, University of New Mexico, Albuquerque, NM 87131, USA
[6]Department of Mathematics, University of Arizona, Tucson, AZ 85721, USA

PML, 0000-0001-6988-5044

A potential motion of ideal incompressible fluid with a free surface and infinite depth is considered in two-dimensional geometry. A time-dependent conformal mapping of the lower complex half-plane of the auxiliary complex variable w into the area filled with fluid is performed with the real line of w mapped into the free fluid's surface. The fluid dynamics can be fully characterized by the motion of the complex singularities in the analytical continuation of both the conformal mapping and the complex velocity. We consider the short branch cut approximation of the dynamics with the small parameter being the ratio of the length of the branch cut to the distance between its centre and the real line of w. We found that the fluid dynamics in that approximation is reduced to the complex Hopf equation for the complex velocity coupled with the complex transport equation for the conformal mapping. These equations are fully integrable by characteristics producing the infinite family of solutions, including moving square root branch points and poles. These solutions involve practical initial conditions resulting in jets

THE ROYAL SOCIETY PUBLISHING

© 2021 The Author(s) Published by the Royal Society. All rights reserved.

and overturning waves. The solutions are compared with the simulations of the fully nonlinear Eulerian dynamics giving excellent agreement even when the small parameter approaches about one.

1. Introduction and basic equations

We consider a two-dimensional potential motion of ideal incompressible fluid with the free surface of infinite depth in the gravity field g as schematically shown in figure 1*a*. Fluid occupies the infinite region $-\infty < x < \infty$ in the horizontal direction x and extends down to $y \to -\infty$ in the vertical direction y. We assume that there is no dependence on the third spatial dimension, i.e. the fluid motion is exactly two dimensional. The bulk of fluid is at rest, i.e. there is no motion of fluid both at $|x| \to \pm\infty$ and $y \to -\infty$.

We use a time-dependent conformal mapping

$$z(w,t) = x(w,t) + \mathrm{i}y(w,t) \tag{1.1}$$

of the lower complex half-plane $\mathbb{C}^-$ of the auxiliary complex variable

$$w \equiv u + \mathrm{i}v, \quad -\infty < u < \infty, \tag{1.2}$$

into the area in (x,y) plane occupied by the fluid. Here, the real line $v = 0$ is mapped into the fluid free surface (figure 1) and $\mathbb{C}^-$ is defined by the condition $-\infty < v \le 0$. Then the time-dependent fluid free surface is represented in the parametric form as

$$x = x(u,t), \quad \text{and} \quad y = y(u,t). \tag{1.3}$$

We assume a decay of perturbation of fluid beyond a flat surface $y \equiv 0$ at $x(u,t) \to \pm\infty$ which requires that

$$z(w,t) \to w + o(1) \quad \text{for } |w| \to \infty,\ w \in \mathbb{C}^-, \tag{1.4}$$

where $o(1)$ means a vanishing contribution in that limit $|w| \to \infty$. The conformal mapping (1.1) implies that $z(w,t)$ is the analytic function of $w \in \mathbb{C}^-$ and

$$z_w \neq 0 \quad \text{for any } w \in \mathbb{C}^-, \tag{1.5}$$

where subscripts here and below means partial derivatives, $z_w \equiv \partial z(w,t)/\partial w$ etc.

Potential fluid motion means that a velocity $\mathbf{v}$ of fluid is determined by a velocity potential $\Phi(\mathbf{r},t)$ as $\mathbf{v} = \nabla\Phi$ with $\nabla \equiv (\partial/\partial x, \partial/\partial y)$. The incompressibility condition $\nabla \cdot \mathbf{v} = 0$ results in the Laplace equation

$$\nabla^2\Phi = 0 \tag{1.6}$$

inside fluid, i.e. Φ is the harmonic function inside fluid. Equation (1.6) is supplemented with a decaying boundary condition (BC) at infinity,

$$\nabla\Phi \to 0 \quad \text{for } |x| \to \infty \text{ or } y \to -\infty, \tag{1.7}$$

which can be replaced without loss of generality by a zero Dirichlet BC

$$\Phi \to 0 \quad \text{for } |x| \to \infty \text{ or } y \to -\infty. \tag{1.8}$$

The harmonic conjugate of Φ is a stream function Θ defined by

$$\Theta_x = -\Phi_y \quad \text{and} \quad \Theta_y = \Phi_x. \tag{1.9}$$

Similar to equation (1.8), we set without loss of generality a zero Dirichlet BC for Θ as

$$\Theta \to 0 \quad \text{for } |x| \to \infty \text{ or } y \to -\infty. \tag{1.10}$$

We define a complex velocity potential $\Pi(z,t)$ as

$$\Pi = \Phi + \mathrm{i}\Theta, \tag{1.11}$$

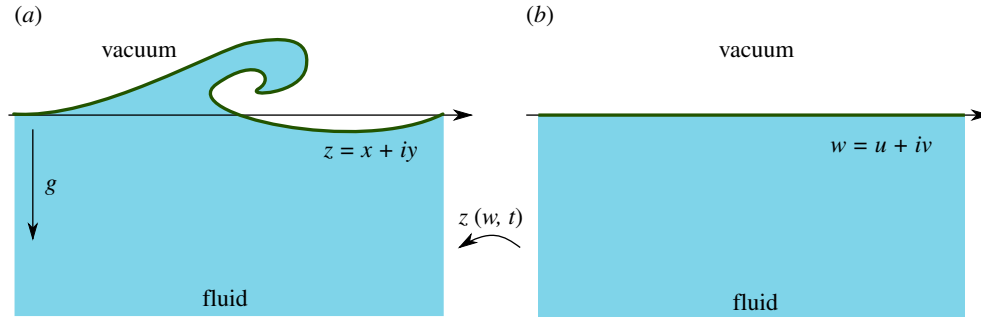

Figure 1. Shaded area represents the domain occupied by fluid both in the physical plane $z = x + iy$ (*a*) and in the plane $w = u + iv$ (*b*). Thick solid lines correspond to the fluid's free surface. Gravity is pointing downwards, i.e. in the direction $-y$ on (*a*). (Online version in colour.)

where $z = x + iy$ is the complex coordinate. Then equation (1.9) turn into Cauchy–Riemann equations resulting in the analyticity of $\Pi(z,t)$ in the domain of z plane occupied by the fluid. A physical velocity with the components v_x and v_y (in x and y directions, respectively) is obtained from Π as $\mathrm{d}\Pi/\mathrm{d}z = v_x - iv_y$. The conformal mapping (1.1) ensures that the function $\Pi(z,t)$ (1.11) transforms into $\Pi(w,t)$ which is the analytic function of w for $w \in \mathbb{C}^-$ (in the bulk of fluid). Here and below, we abuse the notation and use the same symbols for functions of either w or z (in other words, we assume that e.g. $\tilde{\Pi}(w,t) = \Pi(z(w,t),t)$ and remove˜sign). The conformal transformation (1.1) also results in Cauchy–Riemann equations $\Theta_u = -\Phi_v$, $\Theta_v = \Phi_u$ in w plane.

BCs at the free surface are time-dependent and consist of kinematic and dynamic BCs. A kinematic BC states that the free surface moves together with fluid particles located at that surface, i.e. there is no separation of fluid particles from the free surface. For mathematical formulation, we look at the normal component of velocity v_n (normal to the free surface) of such fluid particles. Motion of the free surface is determined by a time derivative of the parametrization (1.3) so the kinematic BC is given by a projection into the normal direction as

$$\mathbf{n} \cdot (x_t, y_t) = v_n \equiv \mathbf{n} \cdot \nabla\Phi|_{x=x(u,t),y=y(u,t)}, \tag{1.12}$$

where $\mathbf{n} = (-y_u, x_u)/(x_u^2 + y_u^2)^{1/2}$ is the outward unit normal vector to the free surface and subscripts here and below means partial derivatives, $x_t \equiv \partial x(u,t)/\partial t$, etc.

A dynamic BC is given by the time-dependent Bernoulli equation (e.g. [1]) at the free surface,

$$\left(\Phi_t + \frac{1}{2}(\nabla\Phi)^2 + gy\right)\Big|_{x=x(u,t),y=y(u,t)} = 0, \tag{1.13}$$

where g is the acceleration due to gravity. Here without loss of generality we assumed that pressure is zero above the free surface (i.e. in vacuum), which is ensured by the zero at the left-hand side (l.h.s.) of equation (1.13). All results below apply both to the surface gravity wave case ($g > 0$) and the Rayleigh–Taylor problem ($g < 0$). We also consider a particular case $g = 0$ when inertia forces well exceed gravity force.

Equations (1.12) and (1.13) together with the analyticity (with respect to the independent variable w) of both $z(w,t)$ and $\Pi(w,t)$ inside fluid as well as the decaying BCs (1.4), (1.8) and (1.10) form a closed set of equations which is equivalent to Euler equations for dynamics of ideal fluid with free surface. The approach of using time-dependent conformal transformation like (1.1) to address free surface dynamics of ideal fluid was exploited by several authors including [2–10]. We follow the approach of [6,11,12] to transform from the unknowns $z(w,t)$ and $\Pi(w,t)$ into the equivalent 'Tanveer–Dyachenko' variables

$$R = \frac{1}{z_w} \tag{1.14}$$

and

$$V = \mathrm{i}\frac{\partial \Pi}{\partial z} = \mathrm{i}R\Pi_w. \tag{1.15}$$

These variables were introduced by Tanveer in [4] for the periodic BC and later independently obtained by Dyachenko in [13] for the decaying BCs (1.4), (1.8) and (1.10) so we refer to these variables as 'Tanveer–Dyachenko variables'. Both

$$R(w,t) \text{ and } V(w,t) \text{ are the analytic functions for } w \in \mathbb{C}^- \tag{1.16}$$

as follows from equation (1.5) and the analyticity of both z and Π for $w \in \mathbb{C}^-$. Then the dynamical equations at the real line $w = u$ take the following complex form [13]:

$$\frac{\partial R}{\partial t} = \mathrm{i}(UR_u - RU_u), \tag{1.17}$$

$$U = \hat{P}^-(R\bar{V} + \bar{R}V), \quad B = \hat{P}^-(V\bar{V}) \tag{1.18}$$

and

$$\frac{\partial V}{\partial t} = \mathrm{i}[UV_u - RB_u] + g(R-1), \tag{1.19}$$

where

$$\hat{P}^- = \frac{1}{2}(1 + \mathrm{i}\hat{H}) \quad \text{and} \quad \hat{P}^+ = \frac{1}{2}(1 - \mathrm{i}\hat{H}) \tag{1.20}$$

are the projector operators of any function $q(u)$ (defined at the real line $w = u$) into functions $q^+(u)$ and $q^-(u)$ analytic in $w \in \mathbb{C}^-$ and $w \in \mathbb{C}^+$, respectively, such that $q = q^+ + q^-$, i.e. $\hat{P}^+(q^+ + q^-) = q^+$ and $\hat{P}^-(q^+ + q^-) = q^-$. Here, we assume that $q(u) \to 0$ for $u \to \pm\infty$. Also the bar means complex conjugation and

$$\hat{H}f(u) = \frac{1}{\pi}\,\text{p.v.}\int_{-\infty}^{+\infty} \frac{f(u')}{u'-u}\mathrm{d}u' \tag{1.21}$$

is the Hilbert transform with p.v. meaning a Cauchy principal value of the integral. See also more discussion of the operators (1.20) in [12]. We refer to equations (1.17)–(1.19) as 'Dyachenko equations' for Tanveer–Dyachenko variables (1.14) and (1.15). Note that [4] also provided the dynamic equations for these variables for the particular case of the periodic BC. These dynamic equations are written in terms of contour integrals with non-polynomial nonlinearities. Although in the periodic case these dynamics equations are equivalent to Dyachenko equations (1.17)–(1.19), we prefer to use the formulation (1.17)–(1.19) because it has only cubic nonlinearity and avoid contour integrals by the projectors (1.20). That formulation is valid both for the periodic BC and decaying BCs (1.4), (1.8) and (1.10).

A complex conjugation $\bar{f}(w)$ of $f(w)$ in equations (1.17)–(1.19) and throughout this paper is understood as applied with the assumption that $f(w)$ is the complex-valued function of the real argument w even if w takes the complex values so that

$$\bar{f}(w) \equiv \overline{f(\bar{w})}. \tag{1.22}$$

That definition ensures the analytical continuation of $f(w)$ from the real axis $w = u$ into the complex plane of $w \in \mathbb{C}$. Following [14], we consider an analytical continuation of the functions R and V into the Riemann surfaces which we call by $\Gamma_R(w)$ and $\Gamma_V(w)$, respectively.

The decaying BCs (1.4), (1.8) and (1.10) imply that

$$R(w,t) \to 1, \ V(w,t) \to 0 \quad \text{for } |\mathrm{Re}(w)| \to \infty \text{ or } \mathrm{Im}(w) \to -\infty. \tag{1.23}$$

Also in §3, we consider the periodic BCs which are still decaying deep inside the fluid as

$$\left.\begin{aligned} &R(w+\lambda,t) = R(w,t), \quad V(w+\lambda,t) = V(w,t) \\ \text{and} \quad &R(w,t) \to 1, \quad V(w,t) \to 0 \quad \text{for } \mathrm{Im}(w) \to -\infty, \end{aligned}\right\} \tag{1.24}$$

where the spatial period λ can be set to 2π without the loss of generality.

The variables R and V (1.14) and (1.15) include only a derivative of the conformal mapping (1.1) and the complex potential Π over w while $z(w,t)$ and $\Pi(w,t)$ are recovered from solution of

these equations as $z = \int (1/R)\,\mathrm{d}w$ and $\Pi = -\mathrm{i}\int (V/R)\,\mathrm{d}w$. It provides a freedom of adding arbitrary functions of time to both $z(w,t)$ and $\Pi(w,t)$. Such addition is not physically important for $\Pi(w,t)$ because it does not change fluid velocity while the addition to $z(w,t)$ changes the location of the free surface. The freedom in the real part x is removed if one notices that generally for the decaying BCs (1.23) $x(u,t) \to u + x_0$ for $|u| \to \infty$ and we choose the constant x_0 to be zero according to equation (1.4). The freedom in the imaginary part y is removed from equation (1.4) by setting that $y(u,t) \to 0$ for $|u| \to \infty$.

For the periodic BCs (1.24), we remove the freedom in x by setting that

$$x(\pi, t) = \pi. \tag{1.25}$$

The freedom in the imaginary part y is removed by ensuring the conservation of the total mass of the fluid. That conservation is expressed through the time independence of the following integral (e.g. [12])

$$M = \int_{-\pi}^{\pi} y(u,t) x_u(u,t)\,\mathrm{d}u. \tag{1.26}$$

Without loss of generality, we set $M = 0$, which corresponds to the zero mean level of the fluid in the vertical direction. E.g. the flat free surface would correspond to $y \equiv 0$. Respectively, while recovering $z(w,t)$ from $R(w,t)$ for the periodic BCs we use that $M = 0$.

Reference [14] found that the system (1.14)–(1.19) has an arbitrary number of pole solutions for z_w and Π_w. These poles are located for $w \in \mathbb{C}^+$, i.e. in the analytical continuation of z_w and Π_w to the area outside of the fluid domain. These pole solutions allowed us to identify the existence of multiple nontrivial integrals of motion (beyond the natural integrals like the Hamiltonian and the horizontal momentum), see [12] for details. Many of these integrals commute with respect to the non-canonical Poisson bracket found in [11,12]. It was suggested in [14] that the existence of such commuting integrals of motion might be a sign of the Hamiltonian integrability of the free surface hydrodynamics. It is well established (e.g. [12,15–32]) that the system of the type (1.17)–(1.19) and its different generalizations also have solutions with branch points located for $w \in \mathbb{C}^+$. Generally, we expect coexistence of poles and branch points at different locations of $w \in \mathbb{C}^+$, see [14] for numerical examples. Also [15] demonstrated that purely rational solutions of the system (1.17)–(1.19) are not very likely for the decaying BCs (1.23). In particular, it was proven in [15] that the rational solutions with the second and/or first-order poles are impossible to survive with dynamics for any finite time duration, i.e. they are not persistent with time evolution.

The plethora of possible analytic solution makes it very important to find a tool to construct analytical solutions involving both branch points and poles. In this paper, we develop such a tool in the approximation of a short branch cut. Such approximations assume that the distance between the most remote branch points is much smaller than the distances from these points to the real line. Then the fluid dynamics is shown to be reduced to the complex Hopf equation for the complex velocity coupled with the complex transport equation for the conformal mapping. These equations are fully integrable by characteristics producing the infinite family of solutions including the pairs of moving square root branch points. We also provide an example of the excellent performance of the solution obtained in that approximation in comparison with numerical solutions of the system (1.17)–(1.19) even when the length of the branch cut becomes comparable with its distance to the real line.

The plan of the paper is the following. In §2, we derive the equations of the short branch cut approximation from the system (1.17)–(1.19). The applicability condition of that approximation is also established. After that we show that these equations in the moving complex frame are reduced to the fully integrable complex Hopf equation for the complex velocity $V(w,t)$ and the transport equation for $z(w,t)$. Section 3 develops the short branch cut approximation for the spatially periodic case of BCs (1.24). Section 4 provides a comparison of the analytical solutions of §3 with the full numerical solution of equations (1.17)–(1.19) and (1.24). Section 5 gives a summary of obtained results and discussion of future directions.

2. Short branch cut approximation and square root singularity solutions

In this section, we derive the dynamical equations of the short branch cut approximation and establish their integrability in characteristics in §2a as well as provide particular solutions in §2b.

(a) Short branch cut approximation

Consider the branch cut γ connecting branch points at $w=a(t)\in\mathbb{C}^+$ and $w=b(t)\in\mathbb{C}^+$. The branch cut is called short one if its distance to the real axis, $\min(|\mathrm{Im}(a)|,|\mathrm{Im}(b)|)$, is large compared with $|a-b|$. It allows to define a small parameter ϵ as follows:

$$\epsilon\equiv|a-b|/\min(|\mathrm{Im}(a)|,|\mathrm{Im}(b)|)\ll 1. \tag{2.1}$$

We neglect other singularities/branch cuts in R and V by assuming that they either identically zero or give small contribution at the real axis $w=u$. Then we define

$$\left.\begin{aligned} R(w,t)-1&=\int_a^b\frac{\tilde{R}(w',t)\,\mathrm{d}w'}{w-w'}\\ \text{and}\qquad V(w,t)&=\int_a^b\frac{\tilde{V}(w',t)\,\mathrm{d}w'}{w-w'}, \end{aligned}\right\} \tag{2.2}$$

where $\tilde{R}(w',t)$ and $\tilde{V}(w',t)$ are densities along branch cut such that the jump of R across branch cut at $w=w'$ is $2\pi\mathrm{i}\tilde{R}(w',t)$ and similar the jump for V is $2\pi\mathrm{i}\tilde{V}(w',t)$ as follows from the Sokhotskii–Plemelj theorem (e.g. [33,34]). Integration in equations (2.2) is taken over any contour which is a simple arc in $\mathbb{C}^+$ connecting $w=a$ and $w=b$. This contour defines a branch cut. There is a freedom in choice of that branch cut connecting two branch points $w=a$ and $w=b$. We however assume that the arclength of the branch cut is of the same order of magnitude as $|a-b|$, i.e. that arclength is not very much different from the length of the segment of the straight line connecting $w=a$ and $w=b$. Also $\tilde{R}(w',t)$ and $\tilde{V}(w',t)$ are assumed to be the continuous functions of w'. Also $\tilde{R}(w',t)$ and $\tilde{V}(w',t)$ can be zero at some parts of the contour. The functions $\bar{R}$ and $\bar{V}$ are given by

$$\left.\begin{aligned} \bar{R}(w,t)-1&=\int_{\bar{a}}^{\bar{b}}\frac{\bar{\tilde{R}}(\bar{w}',t)\,\mathrm{d}\bar{w}'}{w-\bar{w}'}\\ \text{and}\qquad \bar{V}(w,t)&=\int_{\bar{a}}^{\bar{b}}\frac{\bar{\tilde{V}}(\bar{w}',t)\,\mathrm{d}\bar{w}'}{w-\bar{w}'}, \end{aligned}\right\} \tag{2.3}$$

with the contour $\bar{\gamma}$ connecting $w=\bar{a}$ and $w=\bar{b}$ being the reflection of the contour of equation (2.2) with respect to the real axis $w=\mathrm{Re}(w)$.

Functions $U(w,t)$ and $B(w,t)$ can be rewritten as

$$\left.\begin{aligned} U&=R\bar{V}+\bar{R}V-\hat{P}^+(R\bar{V}+\bar{R}V)\\ \text{and}\qquad B&=V\bar{V}-\hat{P}^+(V\bar{V}), \end{aligned}\right\} \tag{2.4}$$

where we used the definition (1.20) to represent $\hat{P}^-$ as $\hat{P}^-=1-\hat{P}^+$. Because $\hat{P}^+f$ is analytic for $w\in\mathbb{C}^+$ for any function f, as well as both $\bar{R}$ and $\bar{V}$ are analytic for $w\in\mathbb{C}^+$ according to the definition (1.22), we conclude from equation (2.4) that both U and B have a branch cut γ connecting $w=a$ and $w=b$ inherited from branch cut of R and V. Then similar to equations (2.2), we represent $U(w,t)$ and $B(w,t)$ through the integrals of the densities $\tilde{U}(w',t)$ and $\tilde{B}(w',t)$ along the branch cut as

$$\left.\begin{aligned} U(w,t)&=\int_a^b\frac{\tilde{U}(w',t)\,\mathrm{d}w'}{w-w'}\\ \text{and}\qquad B(w,t)&=\int_a^b\frac{\tilde{B}(w',t)\,\mathrm{d}w'}{w-w'}. \end{aligned}\right\} \tag{2.5}$$

Using equations (2.2) and (2.3), a calculation of the projectors in the definitions (1.18) is performed through the partial fractions as follows:

$$\begin{aligned}\hat{P}^-[(R-1)\bar{V}] &= \hat{P}^- \int_a^b \int_{\bar{a}}^{\bar{b}} \frac{\tilde{R}(w'',t)\bar{\tilde{V}}(\bar{w}',t)\,\mathrm{d}w''\mathrm{d}\bar{w}'}{(w-w'')(w-\bar{w}')} \\ &= \hat{P}^- \int_a^b \int_{\bar{a}}^{\bar{b}} \frac{\tilde{R}(w'',t)\bar{\tilde{V}}(\bar{w}',t)\,\mathrm{d}w''\mathrm{d}\bar{w}'}{w''-\bar{w}'} \left(\frac{1}{w-w''} - \frac{1}{w-\bar{w}'}\right) \\ &= \int_a^b \int_{\bar{a}}^{\bar{b}} \frac{\tilde{R}(w'',t)\bar{\tilde{V}}(\bar{w}',t)\,\mathrm{d}w''\mathrm{d}\bar{w}'}{w''-\bar{w}'} \frac{1}{w-w''} \\ &= \int_a^b \frac{\tilde{R}(w'',t)\bar{V}(w'',t)\,\mathrm{d}w''}{w-w''}, \end{aligned} \tag{2.6}$$

where at the last line we used the definition (2.3). Similar to equation (2.6), one obtains that

$$\hat{P}^-[(\bar{R}-1)V] = \int_a^b \frac{\tilde{V}(w'',t)[\bar{R}(w'',t)-1]\mathrm{d}w''}{w-w''} \tag{2.7}$$

and

$$B(w,t) = \hat{P}^-[V\bar{V}] = \int_a^b \frac{\tilde{V}(w'',t)\bar{V}(w'',t)\,\mathrm{d}w''}{w-w''}. \tag{2.8}$$

Equations (1.18), (2.5)–(2.8) result in

$$\tilde{U}(w,t) = \tilde{V}(w,t)\bar{R}(w,t) + \tilde{R}(w,t)\bar{V}(w,t) \tag{2.9}$$

and

$$\tilde{B}(w,t) = \tilde{V}(w,t)\bar{V}(w,t), \tag{2.10}$$

where $w \in \gamma$.

The functions $\bar{R}(w,t)$ and $\bar{V}(w,t)$ are analytic for $w \notin \bar{\gamma}$ including $w \in \mathbb{C}^+$ and they are represented by the convergent Taylor series in the open disc $|w-w_0| < r_d$ with $w_0 \in \gamma$. The radius of convergence r_d is given by distance from w_0 to $\bar{\gamma}$. For the short branch cut $r_d \simeq 2|a| \gg |b-a|$. Without the loss of generality we assume that the centre of branch cut is located at the imaginary axis, i.e. $\mathrm{Re}(a+b) = 0$ and choose $w_0 \in \gamma$ to be also at the imaginary axis, $\mathrm{Re}(w_0) = 0$. E.g. for the simplest choice of branch cut γ to be the segment of straight line connecting $w = a$ and $w = b$, we then obtain that

$$w_0 = \frac{(a+b)}{2}. \tag{2.11}$$

In the short branch cut approximation (2.1), we keep only zeroth order terms in Taylor series for $\bar{R}(w,t)$ and $\bar{V}(w,t)$ and denote

$$R_c(t) \equiv \bar{R}(w_0(t),t) \quad \text{and} \quad V_c(t) \equiv \bar{V}(w_0(t),t). \tag{2.12}$$

Using equations (2.5), (2.9)–(2.12), we then obtain in that approximation that

$$U = RV_c + R_cV - V_c \quad \text{and} \quad B = V_cV. \tag{2.13}$$

More accurate approximation for U and B can be obtained from equations (2.5), (2.9)–(2.12) by taking into account more terms in Taylor series of $\bar{R}(w,t)$ and $\bar{V}(w,t)$ at $w = w_0$ beyond

equation (2.12). For instance, by keeping linear terms,

$$\left.\begin{aligned} &\bar{R}(w,t) \simeq R_c(t) + (w - w_0(t))R_c', \quad R_c' \equiv \frac{\partial}{\partial w} R(w,t)\Big|_{w=w_0} \\ \text{and} \quad &\bar{V}(w,t) \simeq V_c(t) + (w - w_0(t))V_c', \quad V_c' \equiv \frac{\partial}{\partial w} V(w,t)\Big|_{w=w_0}, \end{aligned}\right\} \tag{2.14}$$

we obtain a modification of equation (2.13) as $U \to U + \Delta U$ and $B \to B + \Delta B$, where

$$\left.\begin{aligned} &\Delta U = -\langle \tilde{R} \rangle V_c' + \langle \tilde{V} \rangle R_c' + (w - w_0)[V(w,t)R_c' + (R(\omega,t) - 1)V_c'] \\ \text{and} \quad &\Delta B = -\langle \tilde{V} \rangle V_c' + (w - w_0)V(w,t)V_c'. \end{aligned}\right\} \tag{2.15}$$

Here, $\langle \tilde{R} \rangle \equiv \int_a^b \tilde{R}(w)\,\mathrm{d}w$ and $\langle \tilde{V} \rangle \equiv \int_a^b \tilde{V}(w)\,\mathrm{d}w$. The short branch cut approximation requires that both

$$|\Delta U| \ll |U| \quad \text{and} \quad |\Delta B| \ll |B|. \tag{2.16}$$

Qualitatively it implies that singularities in R and V must not be too strong. For example, if a singularity in R is stronger than in V, as studied in [14], then these conditions require that $|\mathrm{Im}(a)V_c'\tilde{R}| \ll |R_c\tilde{V}|$. We note that the limit of infinitely short branch cut recovers pole solutions of [14].

Any approximation of $\bar{R}(w,t)$ and $\bar{V}(w,t)$ in equations (2.9), (2.10) by polynomials in powers of $w - w_0$ turns Dyachenko equations (1.17)–(1.19) into hyperbolic-type PDEs with variable coefficients both in t and w. In the simplest case of zeroth order polynomials, equations (1.17)–(1.19), (2.13) and conditions (2.16) result in the dynamical equations of the short branch cut approximation,

$$\left.\begin{aligned} &R_t + \mathrm{i}V_c R_u = \mathrm{i}R_c(VR_u - V_u R) \\ \text{and} \quad &V_t + \mathrm{i}V_c V_u = \mathrm{i}R_c V V_u + g(R - 1), \end{aligned}\right\} \tag{2.17}$$

which have variable coefficients $R_c(t)$ and $V_c(t)$ in t only. A more general case of the higher order polynomials, i.e. going beyond the short branch cut approximation implying variable coefficients in w (as exemplified in equation (2.14)), will be considered in the separate paper.

In the complex moving frame,

$$\chi = w - \mathrm{i}\int_0^t V_c(t')\,\mathrm{d}t', \tag{2.18}$$

we obtain from equation (2.17), that

$$\left.\begin{aligned} &R_t = \mathrm{i}R_c(VR_\chi - V_\chi R) \\ \text{and} \quad &V_t = \mathrm{i}R_c V V_\chi + g(R - 1), \end{aligned}\right\} \tag{2.19}$$

where the space derivative is over a new independent variable χ.

We now neglect the term with g in equation (2.19), resulting in

$$R_t = \mathrm{i}R_c(VR_\chi - V_\chi R) \tag{2.20}$$

and

$$V_t = \mathrm{i}R_c V V_\chi, \tag{2.21}$$

which is justified either if $g = 0$ or $|R - 1| \ll 1$. This second condition implies that the free surface is initially nearly flat (this approximation applies only for small enough time while the condition $|R - 1| \ll 1$ remains valid).

Equation (2.21) is decoupled from equation (2.20) and turns into the complex Hopf equation

$$V_\tau = VV_\chi \tag{2.22}$$

under the transformation to the new complex time

$$\tau(t) = \mathrm{i}\int_0^t R_c(t')\,\mathrm{d}t' \tag{2.23}$$

and the, respectively, redefined equation (2.18) as

$$\chi = w - \int_0^\tau \frac{V_c(t(\tau'))}{R_c(t(\tau'))}\mathrm{d}\tau'. \tag{2.24}$$

Under the same transformation (2.23) and (2.24), equation (2.20) turns into

$$R_\tau = VR_\chi - V_\chi R, \tag{2.25}$$

which is convenient to transform back from R (1.14) to z which gives

$$z_\tau = Vz_\chi + c(\tau). \tag{2.26}$$

Equation (2.26) ensures that equation (2.25) is valid for the arbitrary function $c(\tau)$ of τ. To fix that freedom in the choice of $c(\tau)$, we have, similar to the discussion after equation (1.24) in §1, to take into account the decaying BCs (1.4) and (1.23). Using the definitions (2.23) and (2.24), we obtain that a change of independent variables from (χ, τ) to (w, t) in equation (2.29) results in

$$\frac{z_t}{\mathrm{i}R_c} + \frac{V_c}{R_c}z_w = Vz_w + c(\tau(t)). \tag{2.27}$$

Taking the limit $w = u$, $u \to \pm\infty$, one obtains from equation (2.27) and BCs (1.4), (1.23) that

$$c(\tau) = \frac{V_c}{R_c}. \tag{2.28}$$

Respectively, equation (2.26) is reduced to

$$z_\tau = Vz_\chi + \frac{V_c}{R_c}. \tag{2.29}$$

Equations (2.22) and (2.29) are easily integrable. Assume that $F(w)$ and $G(w)$ are arbitrary functions analytic for $w \in \mathbb{C}^-$ such that $F(w) \to 0$ as $w \to \infty$ and $G(w) \to w$ as $w \to \infty$. Then a general solution of system (2.22) and (2.29) is given by

$$V = F(\chi_0) \tag{2.30}$$

and

$$z = G(\chi_0) + \int_0^\tau c(\tau')\,\mathrm{d}\tau', \tag{2.31}$$

where the function $\chi_0(\chi, \tau)$ is determined by the solution of the implicit equation

$$\chi = \chi_0 - F(\chi_0)\tau \tag{2.32}$$

and

$$\int_0^\tau c(\tau')\,\mathrm{d}\tau' = \int_0^\tau \frac{V_c(\tau')}{R_c(\tau')}\,\mathrm{d}\tau' \tag{2.33}$$

as follows from equation (2.28).

Equations (2.30) and (2.32) define a parametric representation of a Riemann surface $\Gamma_V(w)$. If $F(\chi_0)$ is the rational function then $\Gamma_V(w)$ has genus zero at the initial time $t = 0$ (e.g. [35] for definition of genus of surface). For $t > 0$, branch points emerge in $\Gamma_V(w)$ thus making genus non-zero. Branch points on the surface Γ_V are zeros of the derivative $\mathrm{d}\chi/\mathrm{d}\chi_0 = 1 - F'(\chi_0)\tau$. Generally, these zeros are simple. Assume such zero to be located at $\chi_0 = \chi_c$. Then one can write that $\chi = (\chi_0 - \chi_c)^2 h(\chi_0)$, implying a square root branch point on Γ_V (one can solve that implicit equation for $\chi_0(\chi)$ to see that). Here, $h(\chi_0)$ is the analytic function of χ_0 at $\chi_0 = \chi_c$ such that $h(\chi_c) \neq 0$. A

number of such branch points (and, respectively, the number of sheets of $\Gamma_V(w)$) can be arbitrary large depending on the rational function $F(\chi_0)$.

A pair of equations (2.30) and (2.31) give a parametric representation of the 'physical' Riemann surface $G(z)$. This surface is not changing with time meaning that a velocity field of the fantom fluid defined in [14] is time independent. This fact additionally shows that the short branch cut approximation has only a limited range of applicability.

(b) Particular solutions

According to [14,15], equation (2.30) does not allow decaying at $w \to \infty$ solution in terms of rational functions for $t > 0$ because any Nth-order pole in V immediately results in the $2N + 1$ order pole term in the right-hand side (r.h.s.) of equation (2.30) which cannot be balanced by the maximum $N + 1$ pole order term in l.h.s. of equation (2.30). Assume that

$$F(w) = -\frac{A}{w - a_0} = V|_{\tau=0}, \tag{2.34}$$

where A and a_0 are the complex constants such that $a_0 \in \mathbb{C}^+$. This initial condition has a pole at $w = a_0$. Then solving equations (2.32) and (2.34) for χ_0, we obtain that

$$\chi_0 = \frac{\chi + a_0}{2} \pm \sqrt{\frac{(\chi - a_0)^2}{4} - A\tau}, \tag{2.35}$$

which has two square root branch points at

$$\chi = a_0 \pm \sqrt{4A\tau}. \tag{2.36}$$

We choose a branch cut to be the straight line segment of length $|2\sqrt{4A\tau}|$ connecting two branch points (2.36).

Equations (2.23), (2.24), (2.30), (2.32)–(2.35) result in

$$(\chi_0)_\chi = \frac{1}{2} + \frac{\chi - a_0}{4\sqrt{((\chi - a_0)^2/4) - A\tau}} \tag{2.37}$$

and

$$V = \frac{-2A}{\chi - a_0 + \sqrt{(\chi - a_0)^2 - 4A\tau}} = -\frac{\chi - a_0 - \sqrt{(\chi - a_0)^2 - 4A\tau}}{2\tau}, \tag{2.38}$$

where the branch of the square root $\sqrt{\dots}$ is chosen to have $\sqrt{(\chi - a_0)^2} = \chi - a_0$ thus satisfying the initial condition (2.34).

The length of the branch cut according to (2.36) is increasing with time as $2\sqrt{4A\tau}$ and the solution (2.38) remains valid while the short cut approximation (2.1) is valid, i.e.

$$|2\sqrt{4A\tau}| \ll |\mathrm{Im}(a_0)|. \tag{2.39}$$

That condition can be generalized by taking into account equations (2.23) and (2.24).

Equation (2.31) for z depends on the arbitrary function $G(\chi_0)$ so we can immediately construct the infinite set of solutions for z; e.g., choosing

$$G(\xi) = \xi \quad \text{for any } \xi \in \mathbb{C}, \tag{2.40}$$

we obtain from equations (2.31) and (2.35) that

$$z = \frac{\chi + a_0}{2} + \sqrt{\frac{(\chi - a_0)^2}{4} - A\tau} + \int_0^\tau \frac{V_c(\tau')}{R_c(\tau')}\,\mathrm{d}\tau', \tag{2.41}$$

with the same choice of the branch of square root as in equation (2.38). Below in this section, we always assume the same choice of the root. Using the definition (1.14), we obtain from

equation (2.35) that

$$R = \frac{1}{(\chi_0)_\chi G_{\chi_0}(\chi_0)}. \tag{2.42}$$

Equations (2.40)–(2.42) result in

$$R = \frac{2\sqrt{(\chi - a_0)^2 - 4A\tau}}{\chi - a_0 + \sqrt{(\chi - a_0)^2 - 4A\tau}} = \frac{\sqrt{(\chi - a_0)^2 - 4A\tau}(\chi - a_0 - \sqrt{(\chi - a_0)^2 - 4A\tau})}{2A\tau}. \tag{2.43}$$

This case corresponds to $R|_{t=0} \equiv 1$, which is the initially flat free surface evolving from the initial velocity distribution (2.34). A solution with such initial condition was first studied in [36,37] in the approximation of weak nonlinearity. It follows from equation (2.36) that one of two branch points reaches the real line $w = \mathrm{Re}(w)$ in a finite time for a general complex value of the complex constant A (the only exception is $A > 0$ when both branch cuts move horizontally parallel to the real line). It means a formation of singularity on the free surface. However, well before that the condition (2.1) of the applicability of the short branch cut approximation is violated as the lower branch point approaches the real line. In §4 we discuss such type of solution in details for the periodic BCs and compare it with the full numerical solution of Euler equations indicating that the singularity in full equations does reach the real line in a finite time.

We now convert the solution (2.36) for the location of branch points into w plane and the physical time t. The location of $w_0(t)$ (2.11) is determined by taking the midpoint

$$\chi_{\mathrm{mid}} \equiv a_0 \tag{2.44}$$

between the two branch points (2.36) and after that using the definitions (2.23) and (2.24) to shift χ by $\int_0^\tau (V_c(t(\tau')))/(R_c(t(\tau')))\,\mathrm{d}\tau'$ to return from the independent variable χ to w. It gives that

$$w_0(t) = a_0 + \int_0^\tau \frac{V_c(t(\tau'))}{R_c(t(\tau'))}\mathrm{d}\tau'. \tag{2.45}$$

For z, we use the initial condition (2.40) so that

$$R(w,t)|_{t=0} \equiv 1. \tag{2.46}$$

In the simplest approximation of equations (2.23) and (2.24), we set

$$\chi \simeq w - \mathrm{i}V_c(0)t = w + \mathrm{i}\frac{\bar{A}t}{a_0 - \bar{a}_0} \tag{2.47}$$

and

$$\tau \simeq \mathrm{i}R_c(0)t = \mathrm{i}t, \tag{2.48}$$

where we used equations (2.23), (2.34), (2.36), (2.45) and (2.46).

Using equations (2.12), (2.36), (2.47) and (2.48), we obtain the approximate positions of branch points in w as follows

$$w = w_\pm \simeq a_0 \pm \sqrt{4A\mathrm{i}t} - \mathrm{i}\frac{\bar{A}t}{a_0 - \bar{a}_0}. \tag{2.49}$$

It is shown in §4 that the periodic BCs version of equation (2.49) is accurate for the values of t well below the applicability condition (2.39) of the short branch cut approximation. Thus it might be sufficient in many practical calculations to use equation (2.49) instead of more accurate evaluations of integrals in equations (2.23) and (2.24).

As another particular initial shape of surface we choose that

$$G(\xi) = \xi + B\log[\xi - C] \text{ for any } \xi \in \mathbb{C} \quad \text{with } C \neq a_0 \text{ and } \mathrm{Im}(C) > 0, \tag{2.50}$$

where B and C are complex constants. We note that equation (2.50) does not satisfy BC (1.4). That asymptotic deficiency can be fixed if we add the extra term $-B\log[\xi - C_1], \mathrm{Im}(C_1) > 0$ in r.h.s. of equation (2.50), which is however beyond the scope of that paper. By ignoring such a fix we also

neglect the last term in r.h.s. of equation (2.31). Then equations (2.31) and (2.50) imply that at any moment of time τ,

$$z = \chi_0(\chi, \tau) + B \log[\chi_0(\chi, \tau) - C], \tag{2.51}$$

where $\chi_0(\chi, \tau)$ is given by equation (2.35).

Using, equation (2.42), we obtain from equation (2.51) that

$$R = \frac{1}{(\chi_0)_\chi} \frac{\chi_0 - C}{\chi_0 - C + B} = \frac{1}{(\chi_0)_\chi} \left(1 - \frac{B}{\chi_0 - C + B}\right) \tag{2.52}$$

and

$$z_\chi = (\chi_0)_\chi \left(1 + \frac{B}{\chi_0 - C}\right). \tag{2.53}$$

We note that equation (2.50) has the branch cut which extends to the complex infinity. However, the corresponding R at $t = 0$ has only the pose singularity, see equation (2.52). Thus the short branch cut approximation remains valid for the initial condition (2.50) at least for small enough t.

If $C \neq a_0$ then it follows from equation (2.50) that the function z_χ has a simple pole at $\chi_0 = C$. Using equation (2.35), we then obtain that a trajectory of motion of that pole in χ plane is given by

$$\chi = C - \frac{A\tau}{a_0 - C}. \tag{2.54}$$

It follows from equation (2.53) that the residue of z_χ at that point is the integral of motion in χ plane, which is exactly equal to the constant B.

In a similar way, the function R in equation (2.52) has a simple pole at $\chi_0 = C - B$ provided $C - B \neq a_0$. A trajectory of motion of that pole in χ plane is given by

$$\chi = C - B - \frac{A\tau}{a_0 - C + B}. \tag{2.55}$$

However, the residue of that pole is not a constant of motion. We note V is regular at $\chi_0 = C - B$ (because we assumed $C - B \neq a_0$) at least for small enough time. Such local solution (with the pole in R and no pole in V) is compatible with the analysis of [14,15] of the system (1.17)–(1.19), where solutions with the pole in both R and V was excluded while a solution with the pole in R only was allowed.

Another particular case is to set

$$R(w, t = 0) = \frac{B_1}{w - a_0} = R|_{\tau=0}, \tag{2.56}$$

where B_1 is the complex constant. This initial condition has a pole at the same $w = a_0$ as the initial pole in V defined in equation (2.34). Then equations (2.40)–(2.42) result in

$$\begin{aligned} R &= \frac{4B_1\sqrt{(\chi - a_0)^2 - 4A\tau}}{(\chi - a_0 + \sqrt{(\chi - a_0)^2 - 4A\tau})^2} \\ &= \frac{B_1\sqrt{(\chi - a_0)^2 - 4A\tau}(\chi - a_0 - \sqrt{(\chi - a_0)^2 - 4A\tau})^2}{4A^2\tau^2}. \end{aligned} \tag{2.57}$$

The particular solution (2.38), (2.57) recovers the asymptotic result of [5] (Case (a) of §4 of [5]) obtained in that Ref. by the matched asymptotic expansions at $t \to 0$.

Equation (2.57) makes sense locally near the pole position but cannot be valid globally because R must approach 1 as $w \to \infty$. So we provided that case only for the exact comparison with [5].

We however can easily fix that deficiency through the replacement of equation (2.56) by

$$R(w, t=0) = 1 + \frac{B_1}{w - a_0} = R|_{\tau=0}. \tag{2.58}$$

Using equation (1.14), we then obtain that

$$z(w, t=0) = w - B_1 \log(w - a_0 + B_1) \tag{2.59}$$

and, using equations (2.31), (2.35), that

$$z = \frac{\chi + a_0}{2} + \sqrt{\frac{(\chi - a_0)^2}{4} - A\tau} - B_1 \log\left(\frac{\chi - a_0}{2} + \sqrt{\frac{(\chi - a_0)^2}{4} - A\tau} + B_1\right). \tag{2.60}$$

Differentiating equation (2.60) over w and using equation (1.14) results in

$$\begin{aligned} R &= \frac{2\sqrt{(\chi - a_0)^2 - 4A\tau}(2B_1 + \chi - a_0 + \sqrt{(\chi - a_0)^2 - 4A\tau})}{(\chi - a_0 + \sqrt{(\chi - a_0)^2 - 4A\tau})^2} \\ &= \frac{\sqrt{(\chi - a_0)^2 - 4A\tau}(2B_1 + \chi - a_0 + \sqrt{(\chi - a_0)^2 - 4A\tau})(\chi - a_0 - \sqrt{(\chi - a_0)^2 - 4A\tau})^2}{8A^2\tau^2}. \end{aligned} \tag{2.61}$$

Equation (2.57) is recovered from equation (2.61) in the limit $B_1 \to \infty$.

We note that in all particular cases (2.43), (2.57) and (2.61), the series expansion at any of two branch points (2.36) shows that $R = 0$ at these points, which is in the perfect agreement with the analytical results of [15]. We also remind that all these particular cases share the same V from equation (2.38).

To express V and R in all these cases in terms of w and t requires to find expression of χ and τ through w and t using equations (2.23) and (2.24). For that one can use definitions (2.12) with χ_0 determined in terms of χ through equation (2.36). After that a general condition (2.1) can be also verified. We note that all particular examples above correspond to the moving branch points according to equation (2.36). It implies that the condition (2.1) is violated at large times so the short branch cut approximation is valid in all these particular cases only for a finite duration of time.

The second sheet of Riemann surface Γ_V corresponds to the opposite choice of sign in equation (2.35). It means that we have to change the sign in front of each square root in equations (2.38), (2.43), (2.57) and equation (2.61). It immediately implies that $V \to \infty$ and $R \to \infty$ as $\chi \to \infty$ in all these equations for the second (non-physical) sheet of Riemann surface.

In all particular examples in this section, the functions V and R are analytic functions of $\sqrt{(\chi - a_0)^2 - 4A\tau}$, i.e. they are analytic in two sheets of Riemann surface of w. This fact is the result of the approximation (2.17) effectively assuming that both $\tilde{V}$ and $\tilde{R}$ are constant on the branch cut. Going beyond that short cut approximation, we expect that V and R can be analytically continued into a much more complicated Riemann surfaces $\Gamma_V(w)$ and $\Gamma_R(w)$ with the unknown total number of sheets. Our experience with the Stokes wave in [38] suggests that generally the number of sheets is infinite. Some exceptional cases like found in [29,30] have only a finite number of sheets of Riemann surface (these solutions however have diverging values of V and R at $w \to \infty$). We suggest that the detailed study of such many- and infinite-sheet Riemann surfaces is one of the most important goal in free-surface hydrodynamics. This topic is however beyond the scope of this paper. We also note that even in the simplest considered case (2.34), the function R can have the arbitrary number of additional poles and branch points depending on the choice of the function $G(\chi_0)$ in equation (2.30) instead of particular cases considered in this Section.

3. Short branch cut approximation and square root singularity solutions for the periodic case

In this section, we extend the results of §2 into the 2π-periodic BCs (1.24) instead of the decaying BCs (1.23) used in §2. In that periodic case, instead of a single branch cut connecting branch points at $w = a(t) \in \mathbb{C}^+$ and $w = b(t) \in \mathbb{C}^+$ of §2, we consider the periodic sum of branch cuts and use the identity

$$\sum_{n=-\infty}^{\infty} \frac{1}{n+a} = \pi \cot \pi a. \tag{3.1}$$

Then taking the sum over branch cuts amounts to replacing $w - w'$ by $(1/2)\tan[(w-w')/2]$ in the denominators of equation (2.2) and all other similar expressions. In particular, equation (2.2) is replaced by

$$\left.\begin{aligned} R(w,t) - 1 &= \frac{1}{2}\int_a^b \frac{\tilde{R}(w',t)\,\mathrm{d}w'}{\tan[(w-w')/2]} \\ \text{and} \qquad V(w,t) &= \frac{1}{2}\int_a^b \frac{\tilde{V}(w',t)\,\mathrm{d}w'}{\tan[(w-w')/2]}. \end{aligned}\right\} \tag{3.2}$$

Equation (2.3) is replaced by

$$\left.\begin{aligned} \bar{R}(w,t) - 1 &= \frac{1}{2}\int_{\bar{a}}^{\bar{b}} \frac{\bar{\tilde{R}}(\bar{w}',t)\,\mathrm{d}\bar{w}'}{\tan[(w-\bar{w}')/2]} \\ \text{and} \qquad \bar{V}(w,t) &= \frac{1}{2}\int_{\bar{a}}^{\bar{b}} \frac{\bar{\tilde{V}}(\bar{w}',t)\,\mathrm{d}\bar{w}'}{\tan[(w-\bar{w}')/2]} \end{aligned}\right\} \tag{3.3}$$

and equation (2.5) is replaced by

$$\left.\begin{aligned} U(w,t) &= \frac{1}{2}\int_a^b \frac{\tilde{U}(w',t)\,\mathrm{d}w'}{\tan[(w-w')/2]} \\ \text{and} \qquad B(w,t) &= \frac{1}{2}\int_a^b \frac{\tilde{B}(w',t)\,\mathrm{d}w'}{\tan[(w-w')/2]}. \end{aligned}\right\} \tag{3.4}$$

Instead of the partial fractions used in equation (2.6), it is more convenient to use the integral representation of the projector $\hat{P}^-$ (1.20) for the periodic functions (e.g. [39]) which follows from equation (1.21) and the Sokhotskii–Plemelj theorem (e.g. [33,34]) giving that

$$\hat{P}^- f = -\frac{1}{2\pi \mathrm{i}} \sum_{n=-\infty}^{\infty} \int_{-\pi}^{\pi} \frac{f(u')\,\mathrm{d}u'}{u' - u + \mathrm{i}0 + 2\pi n} = -\frac{1}{4\pi \mathrm{i}} \int_{-\pi}^{\pi} \frac{f(u')\,\mathrm{d}u'}{\tan[(u'-u+\mathrm{i}0)/2]}, \tag{3.5}$$

where i0 means $\mathrm{i}\epsilon$, $\epsilon \to 0^+$ and we used the identity (3.1).

Using equations (3.2), (3.3) and (3.4), a calculation of the projectors in the definitions (1.18) is performed through moving the integration contour from $(-\pi, \pi)$ to $(-\pi - \mathrm{i}\infty, \pi - \mathrm{i}\infty)$ together with the identity $\tan(-\mathrm{i}\infty) = -\mathrm{i}$ which give that

$$\begin{aligned} \hat{P}^-[(R-1)\bar{V}] &= \frac{1}{4}\hat{P}^- \int_a^b \int_{\bar{a}}^{\bar{b}} \frac{\tilde{R}(w'',t)\bar{\tilde{V}}(\bar{w}',t)\,\mathrm{d}w''\mathrm{d}\bar{w}'}{\tan[(w-w'')/2]\tan[(w-\bar{w}')/2]} \\ &= -\frac{1}{16\pi \mathrm{i}} \int_{-\pi}^{\pi} \int_a^b \int_{\bar{a}}^{\bar{b}} \frac{\tilde{R}(w'',t)\bar{\tilde{V}}(\bar{w}',t)\,\mathrm{d}w''\mathrm{d}\bar{w}'\mathrm{d}u'}{\tan[(u'-w'')/2]\tan[(u'-\bar{w}')/2]\tan[(u'-w+\mathrm{i}0)/2]} \end{aligned}$$

$$= -\frac{1}{4}\int_a^b\int_{\bar{a}}^{\bar{b}} \frac{\tilde{R}(w'',t)\bar{\tilde{V}}(\bar{w}',t)\,\mathrm{d}w''\mathrm{d}\bar{w}'}{1}$$
$$\times\left(\frac{-1}{2} - \frac{1}{\tan[(w-w'')/2]\tan[(w-\bar{w}')/2]} + \frac{1}{\tan[(\bar{w}'-w'')/2]\tan[(w-\bar{w}')/2]}\right)$$
$$= -\frac{1}{4}\int_a^b\int_{\bar{a}}^{\bar{b}} \frac{\tilde{R}(w'',t)\bar{\tilde{V}}(\bar{w}',t)\,\mathrm{d}w''\mathrm{d}\bar{w}'}{1}$$
$$\times\left(\frac{-1}{2} - \frac{1}{\tan[(w-\bar{w}')/2]}\left[\frac{\tan[(\bar{w}'-w'')/2]-\tan[(w-w'')/2]}{\tan[(w-w'')/2]\tan[(\bar{w}'-w'')/2]}\right]\right)$$
$$= -\frac{1}{4}\int_a^b\int_{\bar{a}}^{\bar{b}} \frac{\tilde{R}(w'',t)\bar{\tilde{V}}(\bar{w}',t)\,\mathrm{d}w''\mathrm{d}\bar{w}'}{1}\left(\frac{1}{2} + \left[\frac{1}{\tan[(w-w'')/2]\tan[(\bar{w}'-w'')/2]}\right]\right)$$
$$= -\frac{1}{8}\int_a^b\int_{\bar{a}}^{\bar{b}} \frac{\tilde{R}(w'',t)\bar{\tilde{V}}(\bar{w}',t)\,\mathrm{d}w''\mathrm{d}\bar{w}'}{1} + \frac{1}{4}\int_a^b\int_{\bar{a}}^{\bar{b}} \frac{\tilde{R}(w'',t)\bar{\tilde{V}}(\bar{w}',t)\,\mathrm{d}w''\mathrm{d}\bar{w}'}{\tan[(w-w'')/2]\tan[(w''-\bar{w}')/2]}, \tag{3.6}$$

where we used the following trigonometric identity

$$\cot(a-b) = \frac{1+\tan a\tan b}{\tan a - \tan b},$$

with $a=(\bar{w}'-w'')/2$, $b=(w-w'')/2$ and $a-b=(\bar{w}'-w)/2$.

Now using the definitions (3.2) and (3.3) in equation (3.6), we obtain that

$$\hat{P}^-[(R-1)\bar{V}] = -\frac{1}{2}[R(-\mathrm{i}\infty,t)-1]\bar{V}(\mathrm{i}\infty,t) + \frac{1}{2}\int_a^b \frac{\tilde{R}(w'',t)\bar{V}(w'',t)\,\mathrm{d}w''}{\tan[(w-w'')/2]}, \tag{3.7}$$

where at the first term in r.h.s. of equation (3.6), we take appropriate limits to use the analyticity of R and $\bar{V}$ as follows: $\tan[(w-w')/2]\to -\mathrm{i}\infty$ as $w\to -\mathrm{i}\infty$ in the first equation (3.2) $\tan[(w-\bar{w}')/2]\to \mathrm{i}\infty$ as $w\to \mathrm{i}\infty$ in the second equation (3.3).

Similar to equation (3.7), one obtains that

$$\hat{P}^-[(\bar{R}-1)V] = -\frac{1}{2}[\bar{R}(\mathrm{i}\infty,t)-1]V(-\mathrm{i}\infty,t) + \frac{1}{2}\int_a^b \frac{\tilde{V}(w'',t)[\bar{R}(w'',t)-1]\mathrm{d}w''}{\tan[(w-w''/2)]} \tag{3.8}$$

and

$$\hat{B}(w,t) = \hat{P}^-[V\bar{V}] = -\frac{1}{2}[\bar{V}(\mathrm{i}\infty,t)]V(-\mathrm{i}\infty,t) + \frac{1}{2}\int_a^b \frac{\tilde{V}(w'',t)\bar{V}(w'',t)\,\mathrm{d}w''}{\tan[(w-w''/2)]}. \tag{3.9}$$

We obtain from equations (1.22) and (1.24) that

$$R(-\mathrm{i}\infty,t)-1 = \bar{R}(\mathrm{i}\infty,t)-1 = \bar{V}(\mathrm{i}\infty,t)] = V(-\mathrm{i}\infty,t) = 0. \tag{3.10}$$

Then equations (1.18), (3.4)–(2.8) and (3.10) result in the same equations (2.9) and (2.10) as for the decaying BCs case (1.23) considered in §2.

Similar to §2, we consider the short branch cut approximation for the periodic case recovering exactly the same equations as (2.12)–(2.27). The only difference in addressing these equations in comparison with §2 is to use the periodic BC (1.24). Respectively, instead of equation (2.28), we have to use the conditions (1.25) and (1.26) to determine $c(\tau)$.

As a particular example, we assume a periodic initial condition

$$F(w) = -\frac{A}{2\tan[(w-a_0)/2]} + \frac{\mathrm{i}A}{2} = V|_{\tau=0}, \tag{3.11}$$

where A and a_0 are complex constants such that $a_0\in\mathbb{C}^+$. This initial condition is the periodic analogue of equation (2.34) with the extra constant term $\mathrm{i}A/2$ added to make sure that $V\to 0$ at $\mathrm{Im}(w)\to -\mathrm{i}\infty$, i.e. the decay of the velocity deep inside fluid. This initial condition has poles at $w=a_0+2\pi n,\ n=0,\pm1,\pm2,\ldots$. In contrast with equations (2.32) and (2.34), equations (2.32) and (3.11) cannot be explicitly solved for χ_0. Thus equations (2.30)–(2.32) provide only the implicit form of the solution for the initial condition (3.11). Note that $c(\tau)$ in this section is generally not given by equation (2.28) but is determined the conditions (1.25) and (1.26).

We can still explicitly obtain that the locations of square root branch points if we differentiate equation (2.32) over χ resulting in

$$1 = (\chi_0)_\chi \left[1 + \frac{\mathrm{d}F(\chi_0)}{\mathrm{d}\chi_0}\tau\right] \tag{3.12}$$

and note $(\chi_0)_\chi$ is singular at the square root branch points (e.g. equation (2.37) in the non-periodic case). It implies from equation (3.12) that

$$1 + \frac{\mathrm{d}F(\chi_0)}{\mathrm{d}\chi_0}\tau = 0 \tag{3.13}$$

at each branch point. Solving equation (3.13), we obtain the location of branch point in χ_0 variable as follows

$$\chi_0 = \chi_{0,\pm} \equiv a_0 \pm 2\arcsin\left(\frac{\sqrt{A\tau}}{2}\right) + 2\pi n, \quad n = 0, \pm 1, \pm 2, \ldots. \tag{3.14}$$

Then using equations (3.11), (3.13) and (3.14), we obtain that the square root branch points are located at

$$\chi = \chi_\pm = a_0 - \frac{\mathrm{i}A\tau}{2} \pm \left[\frac{1}{2}\sqrt{A\tau}\sqrt{4 - A\tau} + 2\arcsin\left(\frac{\sqrt{A\tau}}{2}\right)\right] + 2\pi n, \quad n = 0, \pm 1, \pm 2, \ldots. \tag{3.15}$$

Equation (2.36) is recovered from equation (3.15) at the leading order $O(\tau^{1/2})$ for $A\tau \to 0$ and $n = 0$. Similar to equation (2.36), we choose a branch cut to be the straight line segment of length $|\sqrt{A\tau}\sqrt{4 - A\tau} + 4\arcsin(\sqrt{A\tau}/2)|$ connecting the two branch points (3.15). The location of $w_0(t)$ (2.11) is determined by taking the midpoint

$$\chi_{\mathrm{mid}} \equiv a_0 - \frac{\mathrm{i}A\tau}{2} \tag{3.16}$$

between the two branch points (3.15) and after that using the definitions (2.23) and (2.24) to shift χ by $\int_0^\tau \frac{V_c(t(\tau'))}{R_c(t(\tau'))}\mathrm{d}\tau'$ to return from the independent variable χ to w. It gives that

$$w_0(t) = a_0 - \frac{\mathrm{i}A\tau}{2} + \int_0^\tau \frac{V_c(t(\tau'))}{R_c(t(\tau'))}\mathrm{d}\tau'. \tag{3.17}$$

For z, we use the initial condition (2.40) so that

$$R(w, t)|_{t=0} \equiv 1. \tag{3.18}$$

The length of the branch cut is increasing with time as $\propto \sqrt{\tau}$ at $\sqrt{A\tau}$ according to (3.15) and the solution (2.38) remains valid at least while the short cut approximation (2.1) is valid, i.e.

$$|2\sqrt{4A\tau}| \ll |\mathrm{Im}(a_0)|. \tag{3.19}$$

For comparison with simulations one has to return from the independent variables τ and χ to the original variables t and w using equations (2.23) and (2.24). In the simplest approximation of equations (2.23) and (2.24), we set

$$\begin{aligned}\chi \simeq w - \mathrm{i}V_c(0)t = w - \mathrm{i}\left[-\frac{\bar{A}}{2\tan[(w - \bar{a}_0)/2]} - \frac{\mathrm{i}\bar{A}}{2}\right]\Bigg|_{w=a_0, t=0} \\ \times t = w - \mathrm{i}\left[-\frac{\bar{A}}{2\tan[(a_0 - \bar{a}_0)/2]} - \frac{\mathrm{i}\bar{A}}{2}\right]t\end{aligned} \tag{3.20}$$

and

$$\tau \simeq \mathrm{i} R_c(0) t = \mathrm{i}\, t, \tag{3.21}$$

where we used equations (2.23), (2.36), (3.11), (3.17) and (3.18).

Using equations (2.12), (3.15), (3.20) and (3.21), we obtain the approximate positions of branch points in w as follows

$$w = w_{\pm} \simeq a_0 + \mathrm{i}\left[-\frac{\bar{A}}{2\tan\left[(a_0 - \bar{a}_0)/2\right]} - \frac{\mathrm{i}\bar{A}}{2}\right] t + \frac{At}{2}$$
$$\pm \left[\frac{1}{2}\sqrt{Ait}\sqrt{4 - Ait} + 2\arcsin\left(\frac{\sqrt{Ait}}{2}\right)\right] + 2\pi n, \quad n = 0, \pm 1, \pm 2, \ldots. \tag{3.22}$$

For the precise location of branch points instead of the approximation (3.22), we have to find the dependence of τ on t and χ on w and t using equations (2.23) and (2.24) together with the definitions (2.12) and equation (3.17). These equations are implicit ones. Also one has to find $\chi_0(\chi, \tau)$ from the implicit equations (2.32) and (3.11) to be able to use equations (2.30) and (2.31) for finding V_c and R_c from the definitions (2.12).

Similar to the solutions of §2, the particular solutions considered in this section also have the moving branch points according to equation (3.15). It follows from equation (2.36) that one of two branch points reaches the real line $w = \mathrm{Re}(w)$ in a finite time for a general complex value of the complex constant A. It means a formation of singularity on the free surface. However, well before that the condition (2.1) of the applicability of the short branch cut approximation is violated as the lower branch point approaches the real line.

Similar to the discussion in §2, one can find a wide range of particular solutions for the periodic case of this section based on the general solutions (2.30) and (2.31).

4. Comparison of short branch cut approximation with full numerical solution

In this section, we compare the short branch cut approximation described in the §3 with the full numerical solution of the system (1.17)–(1.19) satisfying the initial conditions (3.11) and (3.18). We assume that there is no gravity ($g = 0$). Both functions $z(w, t)$ and $\Pi(w, t)$ are recovered from the variables R and V by means of the relations (1.14) and (1.15) as discussed in §1, where we assume zero mean fluid (1.26) is at zero.

These initial conditions result in a pair of branch points that move according to equation (3.15). The direction of motion depends on the argument of the complex constant A. In the simulations, we chose three values $A = 1$, $A = \mathrm{i}$ and $A = -\mathrm{i}$. The initial pole of the complex velocity, V, is located at $a_0 = \mathrm{i}$. Generally, A can be the arbitrary complex number and a_0 can be the arbitrary complex number from $\mathbb{C}^+$. Figures 2–5 show the spatial profiles (right panel), and the location of branch points (left panel) for both the branch cut approximation of the §3, and the full numerical solutions. The branch points are located at $w = w_{\pm}(t) \equiv w_{\pm,r}(t) + \mathrm{i}w_{\pm,i}(t)$, where $w_{\pm,r}(t)$ and $w_{\pm,i}(t)$ are real-valued. At each time step, the location is recovered from the numerical simulations by the rational approximation procedure outlined in appendix A. Additionally, $v_c = \mathrm{Im}(w_{-,r}(t))$ can be also determined from the asymptotic of the exponential decay rate of the Fourier coefficients $\hat{z}_k \sim \mathrm{e}^{-v_c|k|}$ of $z(w)$ for $|k| \to \infty$, e.g. [39–41] for more details of that Fourier technique. Equation (3.15) provides the analytic formula for the location of branch points in terms of the τ and χ in the branch cut approximation. However, the dependencies of $\tau(t)$ and $\chi(w, t)$ are given by an implicit relation that follows from equation (3.11). For the sake of convenience, we use the approximate equations (3.20) and (3.21), which result in the explicit expression (3.22) for branch point locations in terms of w and t.

We solve the implicit equations (2.30) and (2.32) for $\chi_0(w, \tau)$ at every instant of time τ to determine the shape of the free surface $x(u, t) + \mathrm{i}y(u, t)$. The extra conditions (1.25) and (1.26) are used to find $c(\tau)$, and a subsequent substitution in equations (2.30), (2.31) and (3.11) gives the shape of the surface $z(u, t)$.

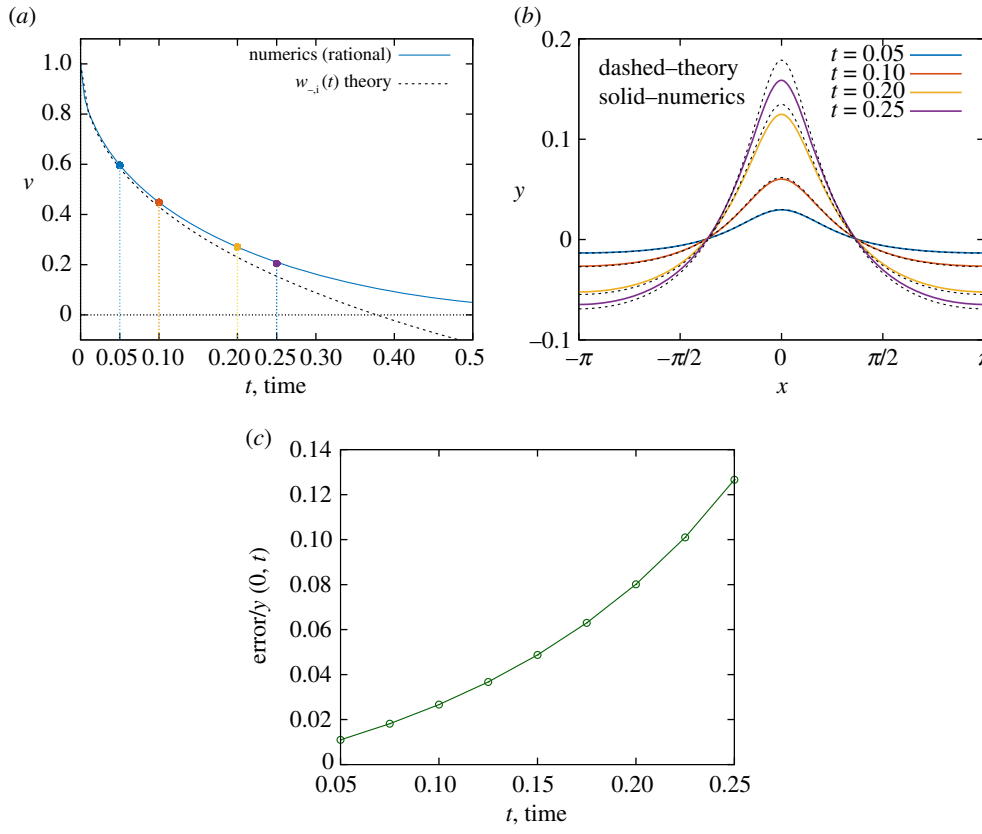

Figure 2. (*a*) The vertical position $v = \mathrm{Im}(w_-(t)) = w_{-,i}(t)$ of the lower branch point versus time t in the simulation with initial conditions (3.11) and (3.18) with $A = \mathrm{i}$ and $a_0 = \mathrm{i}$. The lower branch point location $w_-(t)$ is recovered from the full numerical simulations of equations (1.17)–(1.19) by means of a numerical rational approximation (solid line) compared with its location from the short branch cut approximation (3.15) (dashed line). See appendix A about the rational approximation. The relative error of the theoretic prediction versus numerics is 1.93% at short time $t = 0.05$, about 3.93% at $t = 0.1$, and 15.2% at $t = 0.2$. At $t = 0.05$ and $t = 0.2$, the value of the parameter ϵ introduced in equation (2.1) is 0.61 and 0.89, respectively. These values are well outside the asymptotic condition $\epsilon \ll 1$ when the short branch cut theory is guaranteed to be applicable. (*b*) The spatial profiles of the fluid surface at different times: the result of numerical simulation (solid lines), and the short branch cut approximation (dashed lines). (*c*) The time dependence of the maximum of the error for the surface elevation $y(x, t)$ between the numerical solution and the short branch cut approximation. The maximum of error occurs at $x = 0$ as seen from the surface profiles in (*b*). The error is normalized to the values of $y(0, x)$ from the numerical solution. (Online version in colour.)

The summary of a comparison of the short branch cut approximation and the numerical solutions is given below:

(a) For $A = \mathrm{i}$, both branch points move along the imaginary axis as follows from equation (3.15). The lower branch point, $w_- = \mathrm{i}w_{-,i}(t)$ moves downward from $w = a_0$, and the upper branch point $w_+ = \mathrm{i}w_{+,i}(t)$ is moves upward from $w = a_0$. Figure 2*a* illustrates a dependence of the vertical coordinate of $w_{-,i}(t)$ on time, as determined from the equation (3.15) and the numerical simulations. The positions of branch points are recovered from numerical simulations by the procedure based on a least-squares rational approximation of complex functions and is described in details in [14,39,40]. The vertical coordinate of the lower branch point is also estimated from the asymptotics of the decay rate of the Fourier spectrum giving the same result. Figure 2*b* shows the spatial profiles of the free surface and a comparison of the short branch cut approximation and full

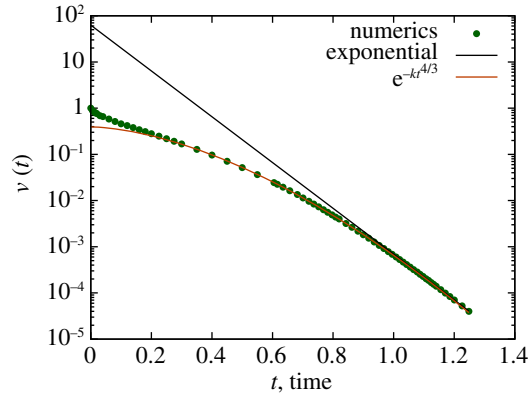

Figure 3. A fit of $v = w_{-,i}(t)$ from figure 2*a* (shown by dots) into the stretched exponent $v = a\,e^{-kt^b}$ with $b = 1$ (black solid line) and $b = 4/3$ (red solid line). It is seen that $b = 4/3$ is much better fit that $b = 1$. Here, $a = 0.39795 \pm 0.01406$ and $k = 6.40096 \pm 0.03348$ are the fitting constants. (Online version in colour.)

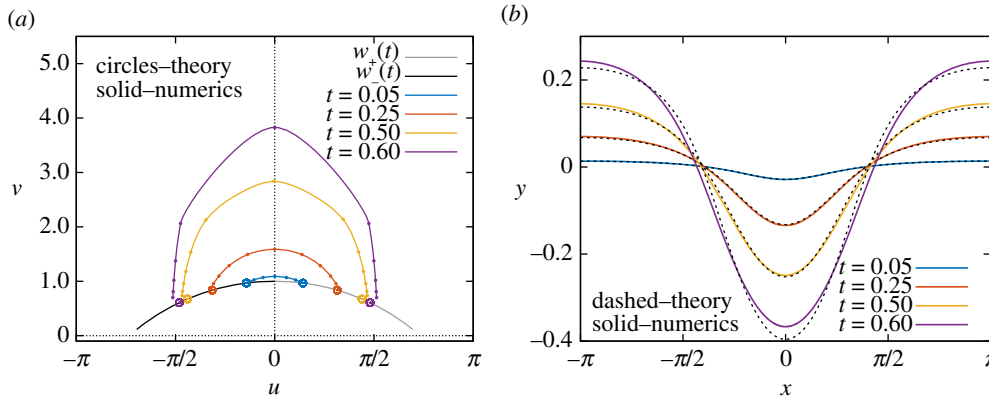

Figure 4. (*a*) The location of the branch cut in the analytical continuation of the complex velocity V (1.15) in the complex plane at several instants of time. The initial conditions are given by (3.11) and (3.18) with $A = -\mathrm{i}$ and $a_0 = \mathrm{i}$. The branch cuts recovered from the numerical simulations of equations (1.17)–(1.19). The filled circles show the positions of poles of rational approximation, and the open circles correspond to the branch point locations given by the analytic formula for $w_{\pm,i}(t)$ from equation (3.15) at the respective time. The solid black lines are the trajectories of $w_{\pm,i}(t)$ from the short cut approximation. The difference in the position of the branch points estimated from the numerical simulation and the short branch cut theory is 2.89% at time $t = 0.05$ ($\epsilon = 0.92$), and is 6.45% at time $t = 0.50$ ($\epsilon = 4.12$). The $w_{\pm,i}(t)$ from equation (3.15) give an excellent estimate for the branch points even for $\epsilon > 1$. (*b*) The spatial profiles of the fluid surface from numerical simulation (solid lines), and short cut approximation (dashed lines). (Online version in colour.)

numerics. It is seen that the spatial profile has a form of jet. Also figure 2*b* shows the time dependence of the maximum error in the surface elevation $y(x, t)$ between the numerical solution and short branch cut approximation.

As discussed in all particular solutions of §§2 and 3, one of the branch points of the analytical solution in the short branch cut reaches the real line $w = \mathrm{Re}(w)$ in a finite time meaning a formation of the singularity of the free surface in a finite time. This is exactly what is seen in figure 2*a*. However, we also see in figure 2*a* that the full numerical solution seems does not produce a finite time singularity. Instead, the singularity appears to occurs at the infinite time $t \to \infty$. To quantify that statement, we performed a fit to the

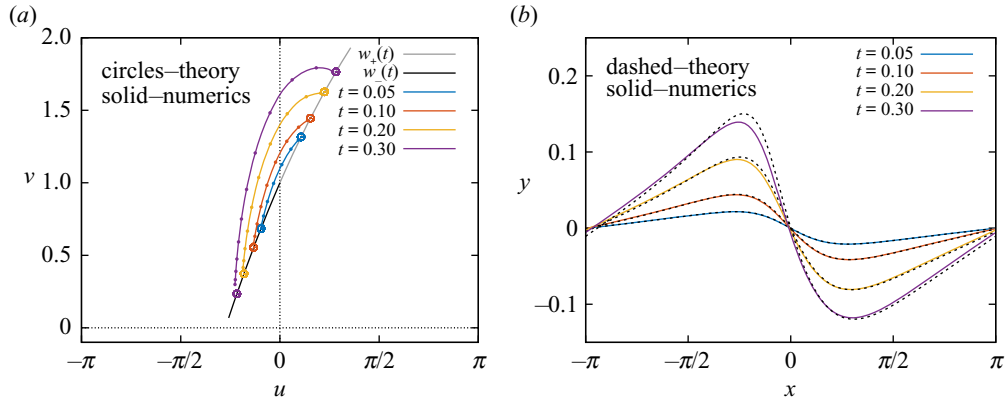

Figure 5. (*a*) The location of the branch cut in the analytical continuation of the complex velocity V (1.15) at different moments of time in the complex plane for initial conditions given by (3.11) and (3.18) with $A = 1$ and $a_0 = \mathrm{i}$. The branch cuts recovered from full numerical simulations of equations (1.17)–(1.19) is given by solid line. The filled circles represent the poles of the rational approximation of the branch cut, and the open circles correspond to the branch point locations $w_{\pm,j}(t)$ from equation (3.15). The grey line passing through $w = \mathrm{i}$ is the trajectory of $w_{\pm,j}(t)$ as obtained from equation (3.15). It is observed that for small time $w_{\pm,j}(t)$ from equation (3.15) approximates the branch points to 3.31% (relative error) at $t = 0.05$ with $\epsilon = 0.68$, and 7.69% (relative error) at $t = 0.25$ with $\epsilon = 1.18$. (*b*) The shape of free surface of the fluid at different times: numerical simulation (solid lines), and the short branch cut approximation (dashed lines). (Online version in colour.)

stretched exponential law $v = a\,\mathrm{e}^{-kt^b}$, where a, b and k are three real fitting constants. We find that $b = 1.333 \simeq 4/3$ provides the best fit as seen in figure 3. Purely exponential fit $b = 1$ is also shown providing not as good fit. Another not as good fit is e.g. $b = 2$, i.e. the Gaussian exponent (not shown in figure 3). The detailed discussion of the topic of finite time singularity is beyond the scope of this paper.

(b) For $A = -\mathrm{i}$, both branch points start to move in the horizontal direction, but unlike the problem on infinite line $-\infty < x < \infty$, the branch points in periodic problem develop vertical speed and approach the real axis. At later times branch cut recovered from numerics is not short thus violating b the short branch cut approximation. However, the positions of branch points recovered from short branch cut approximation agree semi-quantitatively with numerical simulations even at late times. Figure 4*b* shows the spatial profiles of the free surface at different times.

(c) For $A = 1$, both branch points start moving in the complex plane from the initial position at $w = \mathrm{i}a$ as illustrated in the figure 5*a*. Contrary to the other two cases, the positions of the branch points are not symmetric with respect to the imaginary axis. Figure 5*b* shows how the shape of the free surface moves in time with increasing of steepness thus promoting overturning of the wave in a finite time.

We may conclude that the short branch cut approximation gives excellent results up to the values of small parameter $\epsilon \gtrsim 0.9$, well-outside of the applicability region for the short branch cut approximation (2.1).

5. Conclusion and discussion

The main result of this paper is the development of the short branch cut approximation both for the decaying BC (1.23) and the periodic BC (1.24) for free surface hydrodynamics. These equations in the moving complex frame are reduced to the fully integrable complex Hopf equation (2.22) for the complex velocity $V(w, t)$ and the transport equation (2.26) for the conformal map $z(w, t)$. These equations admit the infinite set of solutions easily constructed by the method of characteristics.

Examples of such solutions are provided in §§2 and 3. Section 4 demonstrated the excellent agreement between the analytical solutions of the short branch cut approximation and the full numerical solution of equations (1.17)–(1.19) and (1.24). Examples of jets and overturning waves are shown in these solutions.

The results of §4 appears quite striking because the analytical solutions of the short branch cut approximation agree with relatively good precision in several percents with the solutions of equations (1.17)–(1.19) even when the parameter ϵ introduced in equation (2.1) is not small while the derivation of §§2 and 3 guarantees the applicability of the short branch approximation only for $\epsilon \ll 1$. For future work, we plan to analyse that efficiency of the short branch cut approximation for $\epsilon \gtrsim 1$ by addressing the corrections beyond that approximation outlined in equations (2.14) and (2.13).

Appendix A. Rational approximation for recovery of singularities

In order to recover singularities of the functions R and V in the complex w-plane, we seek a rational approximation of the target function by means of the Alpert–Greengard–Hagström (AGH) originally published in [42], and adapted for the water wave problem in [40]. We outline the general approach to rational approximation of complex functions, and refer the reader to the aforemetioned works for more details. See also [14] for the numerical demonstration of the high efficiency of that method.

AGH algorithm robustly recovers poles in solution while branch cuts are approximated by a set of poles as follows

$$g(\zeta) = \frac{1}{2\pi} \int_C \frac{\rho(\zeta')\,\mathrm{d}\zeta'}{\zeta - \zeta'} \simeq \sum_{n=1}^{N} \frac{\sigma_n}{\zeta - \zeta_n}, \tag{A 1}$$

where the function $g(\zeta)$ has s single branch cut along the contour C in the complex plane of ζ with $\rho(\zeta)$ being a jump of $g(\zeta)$ at the branch cut. The r.h.s. of equation (A 1) approximates $g(\zeta)$ by simple poles located at $\zeta = \zeta_n \in C$, $n = 1, \ldots, N$ with the residues σ_n, $n = 1, \ldots, N$.

Given a 2π-periodic function $f(w)$ on a real periodic interval $w \in [-\pi, \pi]$, we may expand the periodic interval to the real line, $-\infty < \zeta < \infty$, by a coordinate transformation

$$\zeta = \tan \frac{w}{2}, \tag{A 2}$$

which maps the stripe $-\pi < \mathrm{Re}(w) < \pi$ into the complex ζ plane. Also $w \in \mathbb{C}^+(\mathbb{C}^-)$ imply that $\zeta \in \mathbb{C}^+(\mathbb{C}^-)$, see also [40] on more details of the mapping (A 2). ζ variable is convenient to use in AGH algorithm ([40]) which is assumed below.

In the ζ-variable, the function $g(\zeta) = f(w(\zeta)) - f(\pi)$ is defined on the real line and decays to zero as $\xi \to \pm\infty$. The function $g(\zeta)$ is suitable for rational approximation in the ζ-variable, and we seek two polynomials $P(\zeta)$ and $Q(\zeta)$ of degrees N and $N+1$, respectively, such that

$$\epsilon_N \equiv \int_{-\infty}^{+\infty} \left| g(\zeta) - \frac{P(\zeta)}{Q(\zeta)} \right|^2 \mathrm{d}\zeta \to \min, \tag{A 3}$$

where minimization goes over the polynomial coefficients of $P(\zeta)$ and $Q(\zeta)$.

After the optimal polynomials P and Q have been determined, the resulting approximant gives accurate approximation to $g(\zeta)$ on the real line. However, the ratio $P(\zeta)/Q(\zeta)$ defines a meromorphic function in the complex ζ–plane, and its singularities may be determined by seeking the roots ζ_k of $Q(\zeta) = 0$. The residues at the poles are given by $P(\zeta_k)/Q'(\zeta_k)$ and can be used to recover an approximation to the Cauchy type integral as given by equation (A 1).

Data accessibility. The codes used for producing Figures of §4 are publicly available at GitHub digital repository: https://github.com/urrfinjuss/deep-water-full.

Authors' contributions. A.I.D. and V.E.Z. contributed to developing analytical results. P.M.L. and S.A.D. contributed to developing analytical results and numerical simulations. All authors gave final approval for publication and agree to be held accountable for the work performed therein.

Competing interests. We declare we have no competing interests.

Funding. The work of V.E.Z. and A.I.D. was supported by the Russian Science Foundation grant no. 19-72-30028. The work of P.M.L. was supported by the National Science Foundation, grant no. DMS-1814619. The work of V.E.Z. was supported by the National Science Foundation, grant no. DMS-1715323. The work of S.A.D. was supported by the National Science Foundation, grant no. DMS-1716822. We thank support of Russian Ministry of Science and Higher Education grant no. 075-15-2019-1893. Simulations were performed at the Texas Advanced Computing Center using the Extreme Science and Engineering Discovery Environment (XSEDE), supported by NSF grant no. ACI-1053575.

Acknowledgements. P.M.L. would like to thank the Isaac Newton Institute for Mathematical Sciences, Cambridge, for support and hospitality during the programme 'Complex analysis: techniques, applications and computations' where work on this paper was partially undertaken.

References

1. Landau LD, Lifshitz EM. 1989 *Fluid mechanics*, vol. 6, 3rd edn. New York, NY: Pergamon.
2. Ovsyannikov LV. 1973 Dynamics of a fluid, M.A. Lavrent'ev Institute of Hydrodynamics Sib. *Branch USSR Ac. Sci.* **15**, 104–125.
3. Meison D, Orzag S, Izraely M. 1981 Applications of numerical conformal mapping. *J. Comput. Phys.* **40**, 345–360. (doi:10.1016/0021-9991(81)90215-1)
4. Tanveer S. 1991 Singularities in water waves and Rayleigh-Taylor instability. *Proc. R. Soc. Lond. A* **435**, 137–158. (doi:10.1098/rspa.1991.0134)
5. Tanveer S. 1993 Singularities in the classical Rayleigh-Taylor flow: formation and subsequent motion. *Proc. R. Soc. Lond. A* **441**, 501–525. (doi:10.1098/rspa.1993.0076)
6. Dyachenko AI, Kuznetsov EA, Spector M, Zakharov VE. 1996 Analytical description of the free surface dynamics of an ideal fluid (canonical formalism and conformal mapping). *Phys. Lett. A* **221**, 73–79. (doi:10.1016/0375-9601(96)00417-3)
7. Chalikov D, Sheinin D. 1998 Direct modeling of one-dimensional nonlinear potential waves. *Adv. Fluid Mech.* **17**, 207–258.
8. Chalikov D, Sheinin D. 2005 Modeling of extreme waves based on equation of potential flow with a free surface. *J. Comput. Phys.* **210**, 247–273. (doi:10.1016/j.jcp.2005.04.008)
9. Chalikov DV. 2016 *Numerical modeling of sea waves*. Berlin, Germany: Springer.
10. Zakharov VE, Dyachenko AI, Vasiliev OA. 2002 New method for numerical simulation of nonstationary potential flow of incompressible fluid with a free surface. *Eur. J. Mech. B/Fluids* **21**, 283–291. (doi:10.1016/S0997-7546(02)01189-5)
11. Zakharov VE, Dyachenko AI. 2012 Free-surface hydrodynamics in the conformal variables. (http://arxiv.org/1206.2046).
12. Dyachenko AI, Lushnikov PM, Zakharov VE. 2019 Non-canonical Hamiltonian structure and Poisson bracket for two-dimensional hydrodynamics with free surface. *J. Fluid Mech.* **869**, 526–552. (doi:10.1017/jfm.2019.219)
13. Dyachenko AI. 2001 On the dynamics of an ideal fluid with a free surface. *Dokl. Math.* **63**, 115–117.
14. Dyachenko AI, Dyachenko SA, Lushnikov PM, Zakharov VE. 2019 Dynamics of poles in 2D hydrodynamics with free surface: new constants of motion. *J. Fluid Mech.* **874**, 891–925. (doi:10.1017/jfm.2019.448)
15. Lushnikov PM, Zakharov VE. In press. Poles and branch cuts in free surface hydrodynamics. *Water Waves*. (doi:10.1007/s42286-020-00040-y)
16. Moore DW. 1979 The spontaneous appearance of a singularity in the shape of an evolving vortex sheet. *Proc. R. Soc. Lond. A* **365**, 105–119. (doi:10.1098/rspa.1979.0009)
17. Meiron DI, Baker GR, Orszag SA. 1982 Analytic structure of vortex sheet dynamics. Part 1. Kelvin–Helmholtz instability. *J. Fluid Mech.* **114**, 283–298. (doi:10.1017/S0022112082000159)
18. Baker GR, Meiron DI, Orszag SA. 1982 Generalized vortex methods for free-surface flow problems. *J. Fluid Mech.* **123**, 477–501. (doi:10.1017/S0022112082003164)
19. Krasny R. 1986 A study of singularity formation in a vortex sheet by the point–vortex approximation. *J. Fluid Mech.* **167**, 65–93. (doi:10.1017/S0022112086002732)
20. Caflisch R, Orellana O. 1989 Singular solutions and ill–posedness for the evolution of vortex sheets. *SIAM J. Math. Anal.* **20**, 293–307. (doi:10.1137/0520020)
21. Caflisch R, Orellana O, Siegel M. 1990 A localized approximation method for vortical flows. *SIAM J. Appl. Math.* **50**, 1517–1532. (doi:10.1137/0150089)

22. Baker GR, Shelley MJ. 1990 On the connection between thin vortex layers and vortex sheets. *J. Fluid Mech.* **215**, 161–194. (doi:10.1017/S0022112090002609)
23. Shelley MJ. 1992 A study of singularity formation in vortex–sheet motion by a spectrally accurate vortex method. *J. Fluid Mech.* **244**, 493–526. (doi:10.1017/S0022112092003161)
24. Caflisch RE, Ercolani N, Hou TY, Landis Y. 1993 Multi-valued solutions and branch point singularities for nonlinear hyperbolic or elliptic systems. *Commun. Pure Appl. Math.* **46**, 453–499. (doi:10.1002/cpa.3160460402)
25. Baker G, Caflisch RE, Siegel M. 1993 Singularity formation during Rayleigh–Taylor instability. *J. Fluid Mech.* **252**, 51–78. (doi:10.1017/S0022112093003660)
26. Cowley SJ, Baker GR, Tanveer S. 1999 On the formation of Moore curvature singularities in vortex sheets. *J. Fluid Mech.* **378**, 233–267. (doi:10.1017/S0022112098003334)
27. Baker GR, Xie C. 2011 Singularities in the complex physical plane for deep water waves. *J. Fluid Mech.* **685**, 83–116. (doi:10.1017/jfm.2011.283)
28. Zubarev NM, Kuznetsov EA. 2014 Singularity formation on a fluid interface during the Kelvin-Helmholtz instability development. *J. Exp. Theor. Phys.* **119**, 169–178. (doi:10.1134/S1063776114060077)
29. Karabut EA, Zhuravleva EN. 2014 Unsteady flows with a zero acceleration on the free boundary. *J. Fluid Mech.* **754**, 308–331. (doi:10.1017/jfm.2014.401)
30. Zubarev NM, Karabut EA. 2018 Exact local solutions for the formation of singularities on the free surface of an ideal fluid. *JETP Lett.* **107**, 412–417. (doi:10.1134/S0021364018070135)
31. Lushnikov PM, Zubarev NM. 2018 Exact solutions for nonlinear development of a Kelvin-Helmholtz instability for the counterflow of superfluid and normal components of Helium II. *Phys. Rev. Lett.* **120**, 204504. (doi:10.1103/PhysRevLett.120.204504)
32. Lushnikov PM, Zubarev NM. 2019 Explosive development of the Kelvin-Helmholtz quantum instability on the He-II free surface. *J. Exp. Theor. Phys.* **129**, 651–658. (doi:10.1134/S1063776119100157)
33. Gakhov FD. 1966 *Boundary value problems*. New York, NY: Pergamon Press.
34. Polyanin AD, Manzhirov AV. 2008 *Handbook of integral equations: second edition*. Boca Raton, FL: Chapman and Hall/CRC.
35. Dubrovin BA, Fomenko AT, Novikov SP. 1985 *Modern geometry: methods and applications: Part II: the geometry and topology of manifolds*. Berlin, Germany: Springer.
36. Kuznetsov E, Spector M, Zakharov V. 1993 Surface singularities of ideal fluid. *Phys. Lett. A* **182**, 387–393. (doi:10.1016/0375-9601(93)90413-T)
37. Kuznetsov EA, Spector MD, Zakharov VE. 1994 Formation of singularities on the free surface of an ideal fluid. *Phys. Rev. E* **49**, 1283–1290. (doi:10.1103/PhysRevE.49.1283)
38. Lushnikov PM. 2016 Structure and location of branch point singularities for Stokes waves on deep water. *J. Fluid Mech.* **800**, 557–594. (doi:10.1017/jfm.2016.405)
39. Lushnikov PM, Dyachenko SA, Silantyev DA. 2017 New conformal mapping for adaptive resolving of the complex singularities of Stokes wave. *Proc. R. Soc. A* **473**, 20170198. (doi:10.1098/rspa.2017.0198)
40. Dyachenko SA, Lushnikov PM, Korotkevich AO. 2016 Branch cuts of stokes wave on deep water. Part I: numerical solution and Padé approximation. *Stud. Appl. Math.* **137**, 419–472. (doi:10.1111/sapm.12128)
41. Dyachenko SA, Lushnikov PM, Korotkevich AO. 2013 The complex singularity of a Stokes wave. *JETP Lett.* **98**, 675–679. (doi:10.1134/S0021364013240077)
42. Alpert B, Greengard L, Hagstrom T. 2000 Rapid evaluation of nonreflecting boundary kernels for time-domain wave propagation. *SIAM J. Numer. Anal.* **37**, 1138–1164. (doi:10.1137/S0036142998336916)